Electronic Supplementary Material (ESI) for RSC Advances.
This journal is © The Royal Society of Chemistry 2021

Ultrasmall copper nanoclusters with multi-enzyme activities

Yangbin Peng[1,†], Ying Ren[2,†], Hao Zhu[1], Yu An[3], Baisong Chang[*1], Taolei Sun[*1,3]

1. State Key Laboratory of Advanced Technology for Materials Synthesis and Processing, Wuhan University of Technology, Wuhan 430070, PR China

2. Department of Radiology, Shengjing Hospital of China Medical University, Shenyang, 110004, P. R. China

3. School of Chemistry, Chemical Engineering and Life Science, Wuhan University of Technology, Wuhan 430070, PR China

† These authors contributed equally.

Email: chang@whut.edu.cn (B. Chang)

Email: suntl@whut.edu.cn (T. Sun)

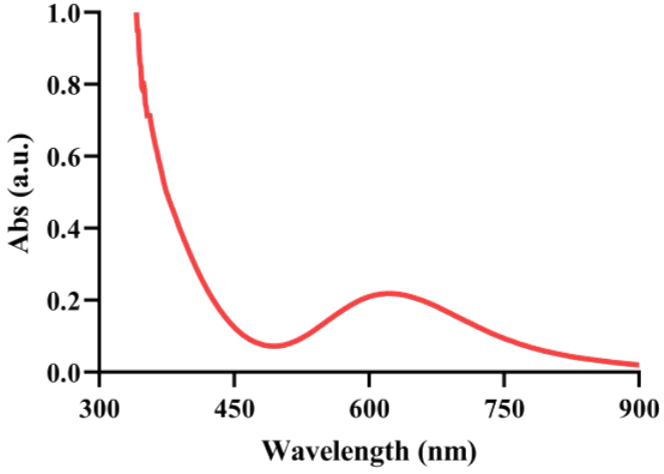

Fig. S1. The UV spectrum of copper nanoparticles with GSH as ligand. Owing to surface plasmon resonance (SPR) excitation or interband transition, nanoparticles show characteristic absorption peaks in the UV spectrum. It can be seen that the as-obtained copper nanoparticles had a broad absorption band centering at 610 nm. As a comparison, no clear absorption bands were observed in the UV spectrum of CuNCs.

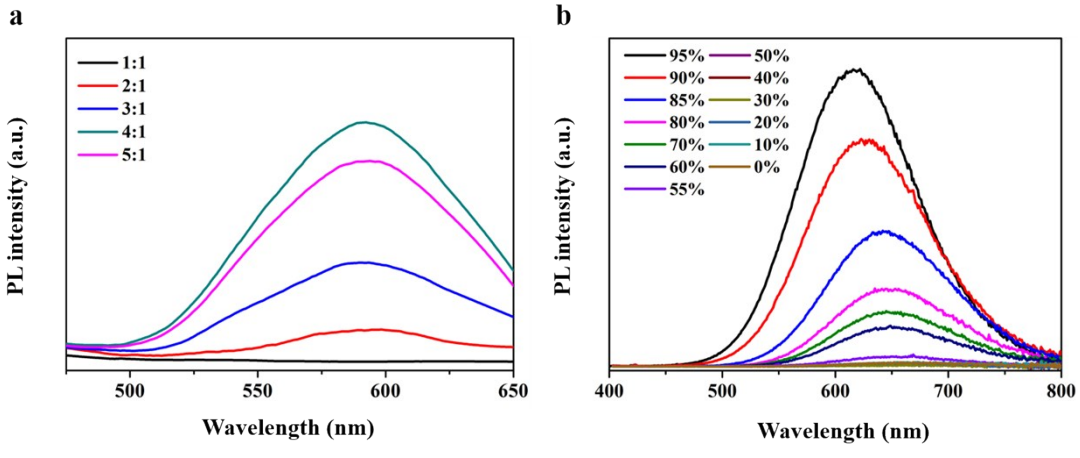

Fig. S2. a) The emission spectra of CuNCs prepared with different ratios of GSH/Cu^{2+}. To determine the optimal synthetic recipes of GSH/Cu^{2+}, 1:1, 2:1, 3:1, 4:1 and 5:1 molar ratios of GSH/Cu^{2+} were investigated. The corresponding emission spectra were recorded. b) The emission spectra of CuNCs in ethanol with different volume ratios of ethanol/water. Upon addition of ethanol, a strong emission peak at ~610 nm was observed, accompanied with the striking enhanced PL intensity.

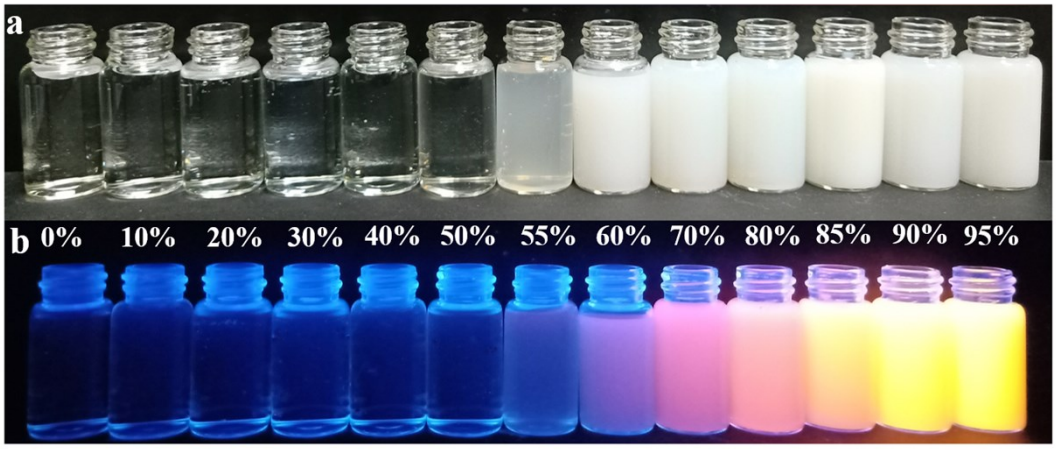

Fig. S3. a) Photos of CuNCs in ethanol/water solution under white light. b) Fluorescent photos of CuNCs in ethanol/water solution under UV irradiation (365 nm). The few-atom CuNCs showed obvious aggregation-induced emission enhancement. With the increase of ethanol concentrations, CuNCs in the solution continued to aggregate, accompanying with the significant increase of fluorescence intensity. The reason for this phenomenon might be ascribed to the changed polarity of solution by adding ethanol. In non-aggregated state, the excited CuNCs can return to the ground state through the vibration or rotation of surface ligand molecules. However, the rotation and vibration of ligand molecules were greatly restricted in the aggregated state. Therefore, the energy of the excited CuNCs will be released in the form of non-radiative transitions, thus showing a strong increase in fluorescence intensity.

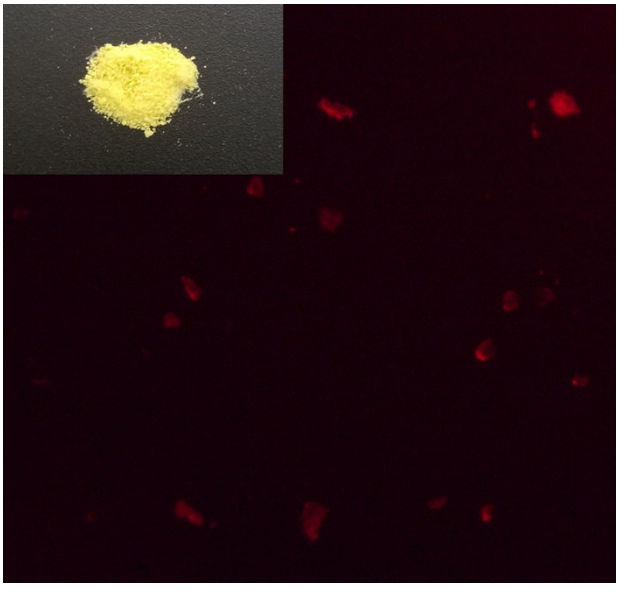

Fig. S4. The photos of CuNCs powder in UV lamp and sunlight (inset).

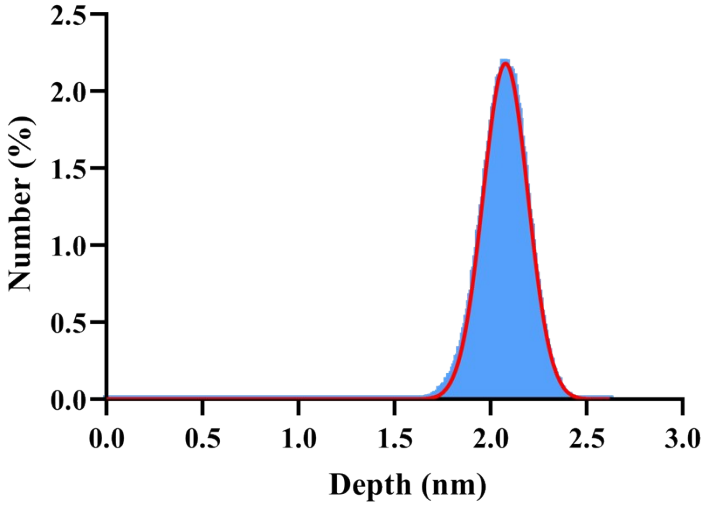

Fig. S5. The size distribution of CuNCs by AFM. AFM results indicated that the average size of the as-prepared CuNCs was less than 2.3 nm.

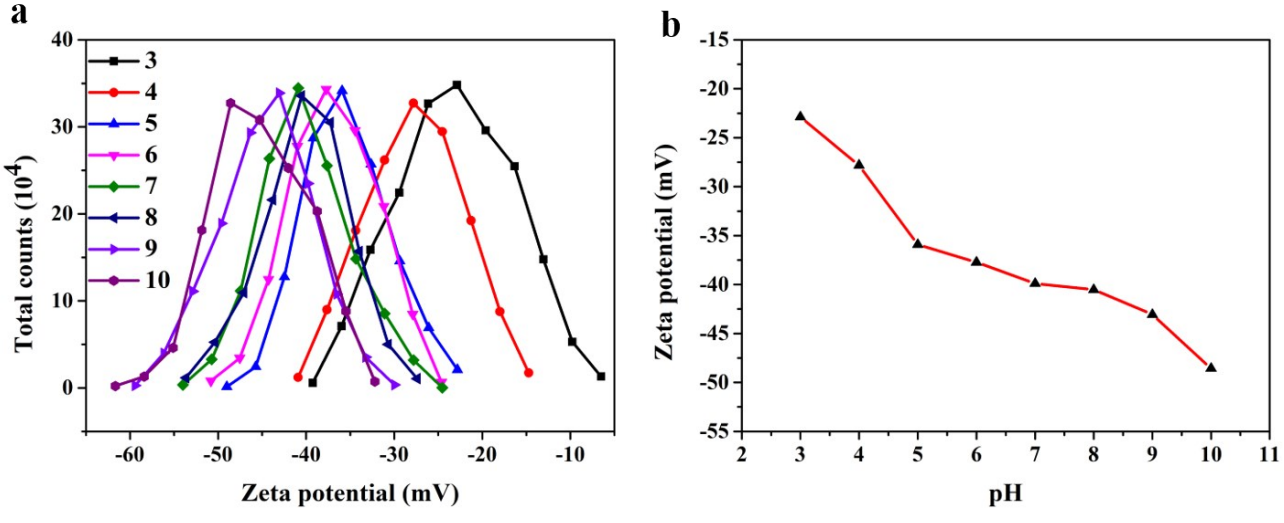

Fig. S6. a, b) Zeta potential of CuNCs in pH 3-10. The Zeta potential values of CuNCs at different pH (3-10) were also measured to evaluate the colloidal stability of CuNCs. It was obvious that the absolute zeta potential values increased with the increase of pH. Especially, when the pH of the solution was greater than 6, the large absolute zeta potential values (above 35 mV) indicated better stability under neutral or alkaline conditions.

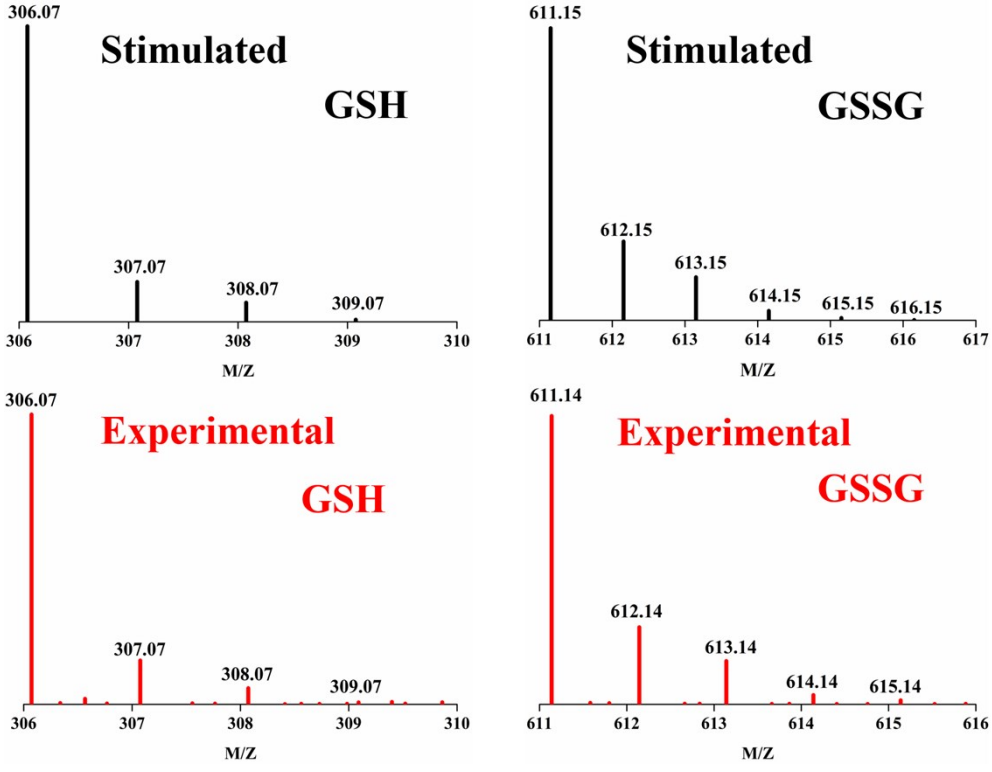

Fig. S7. The experimental (red curve) and simulated (black curve) isotopic patterns of GSH and GSSG.

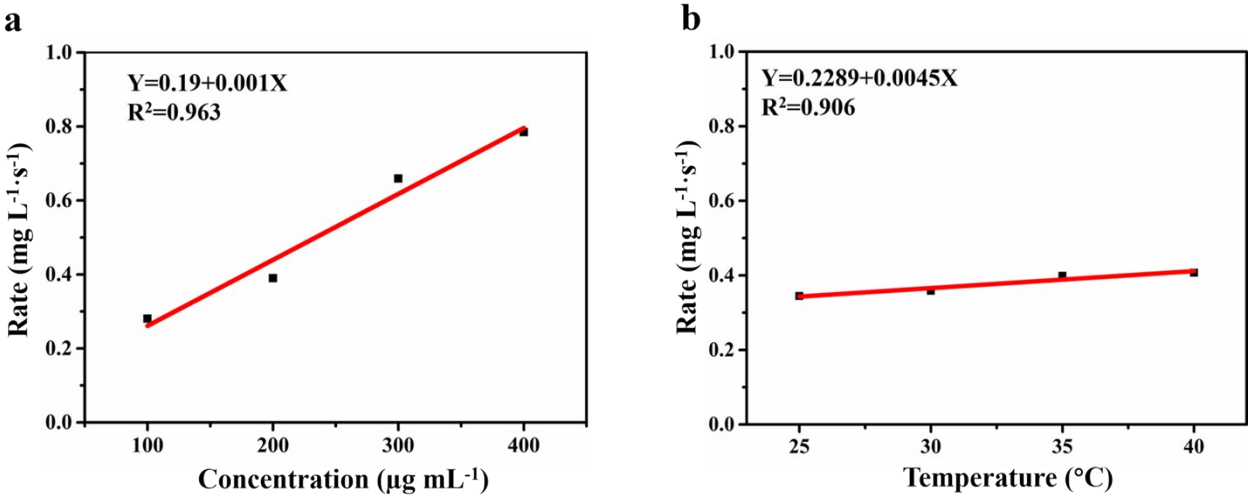

Fig. S8. a, b) The concentration-dependent and temperature-dependent CAT-like activity of CuNCs, showing a linear dependence of the initial rate for reduction of H_2O_2. The reaction mixture contained a fixed concentration of H_2O_2 (10 mM) and different concentration of CuNCs (0-400 μg mL^{-1}) in PBS buffer (10 mM, pH 7.0).

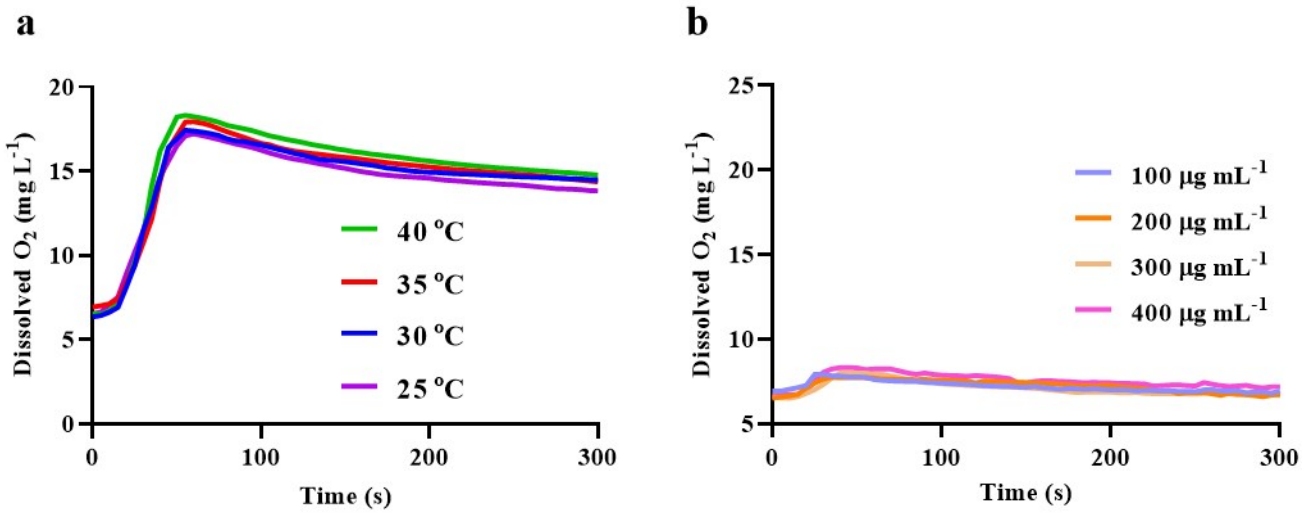

Fig. S9. a) Plot of dissolved O_2 versus time of H_2O_2 (10 mM) in the presence of CuNCs (200 µg mL^{-1}) at different temperatures. b) Plot of dissolved O_2 versus time of H_2O_2 (10 mM) in the presence of GSH (100-400 µg mL^{-1}).

Fig. S10. The photo (left) of H_2O_2 solution in present of CuNCs (100 µg mL^{-1}). The photo (right) of H_2O_2 solution in presence of GSH (100 µg mL^{-1}). The presence of bubbles indicated the catalytic properties of CuNCs.

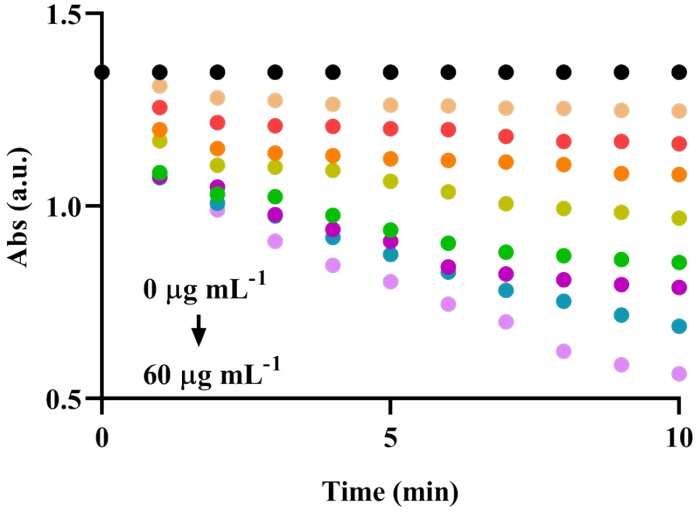

Fig. S11. GPx-like activity of CuNCs. Plot of the absorbance versus time for the reaction of DTNB in the presence of CuNCs (0-60 μg mL^{-1}). The significant decline of absorbance of DTNB in the presence of CuNCs revealed that GSH was catalyzed into GSSG.

All steady-state dynamics measurements were made at 37 °C. By fitting the absorbance data to the Michaelis-Menten equation, which describes the relationship between substrate conversion and substrate concentration of an enzyme, as shown in the following equation.

$$V = \frac{V_{max}[S]}{K_m + [S]}$$

In this equation, V is the conversion rate, V_{max} is the maximum conversion rate, [S] is the concentration of substrate, K_m denotes the affinity of the enzyme to the substrate: a lower K_m value denotes a higher affinity.

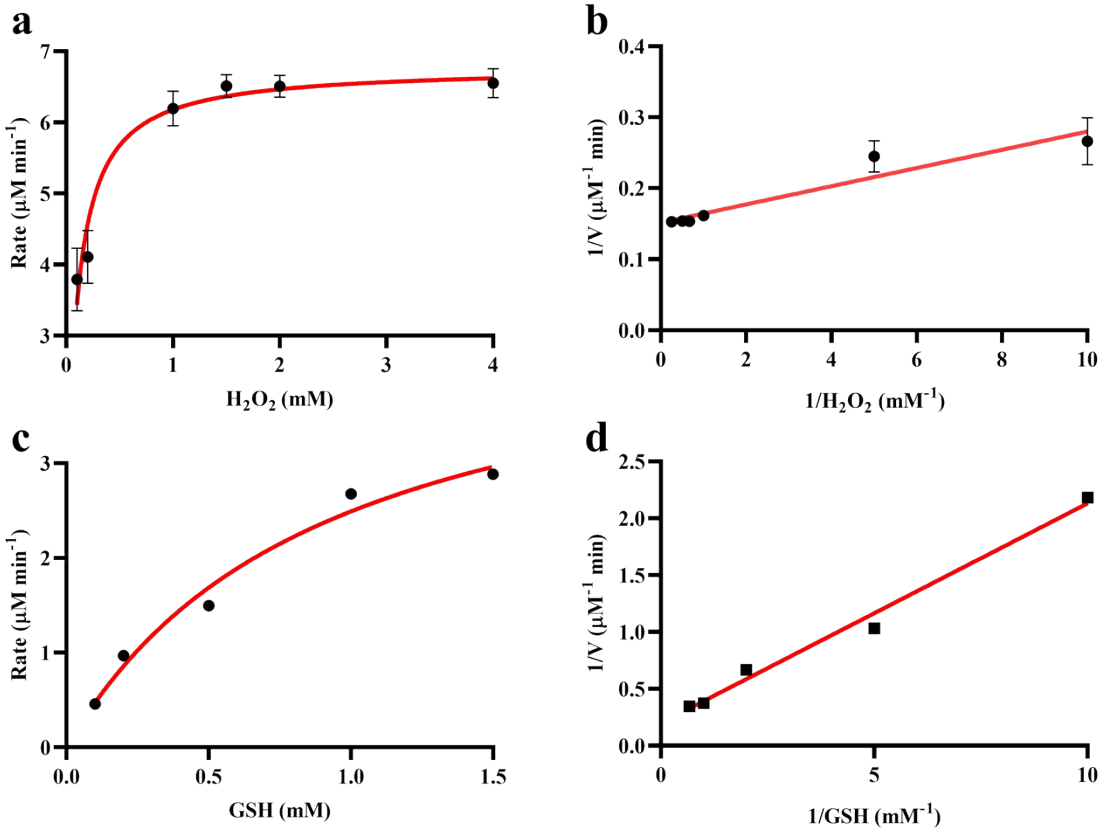

Catalyst	Substance	K_m [mM]	V_{max} [μM min^{-1}]
CuNCs	H_2O_2	0.097	6.781
CuNCs	GSH	0.913	4.766

Fig. S12. The GPx-like activity of the CuNCs. a) Michaelis-Menten and b) corresponding Lineweaver-Burk plot with various concentrations of H_2O_2 (1-4 mM) for the CuNCs. Experimental conditions: DTNB (1 mM), GSH (1 mM), and CuNCs (20 μg mL^{-1}) in PBS (10 mM, pH=7.2) at 37 °C. c) Michaelis-Menten and d) corresponding Lineweaver-Burk plot with various concentrations of GSH (0.1-1.5 mM) for the CuNCs. Experimental conditions: DTNB (1 mM), H_2O_2 (1 mM) and CuNCs (20 μg mL^{-1}) in PBS (10 mM, pH=7.2) at 37 °C.

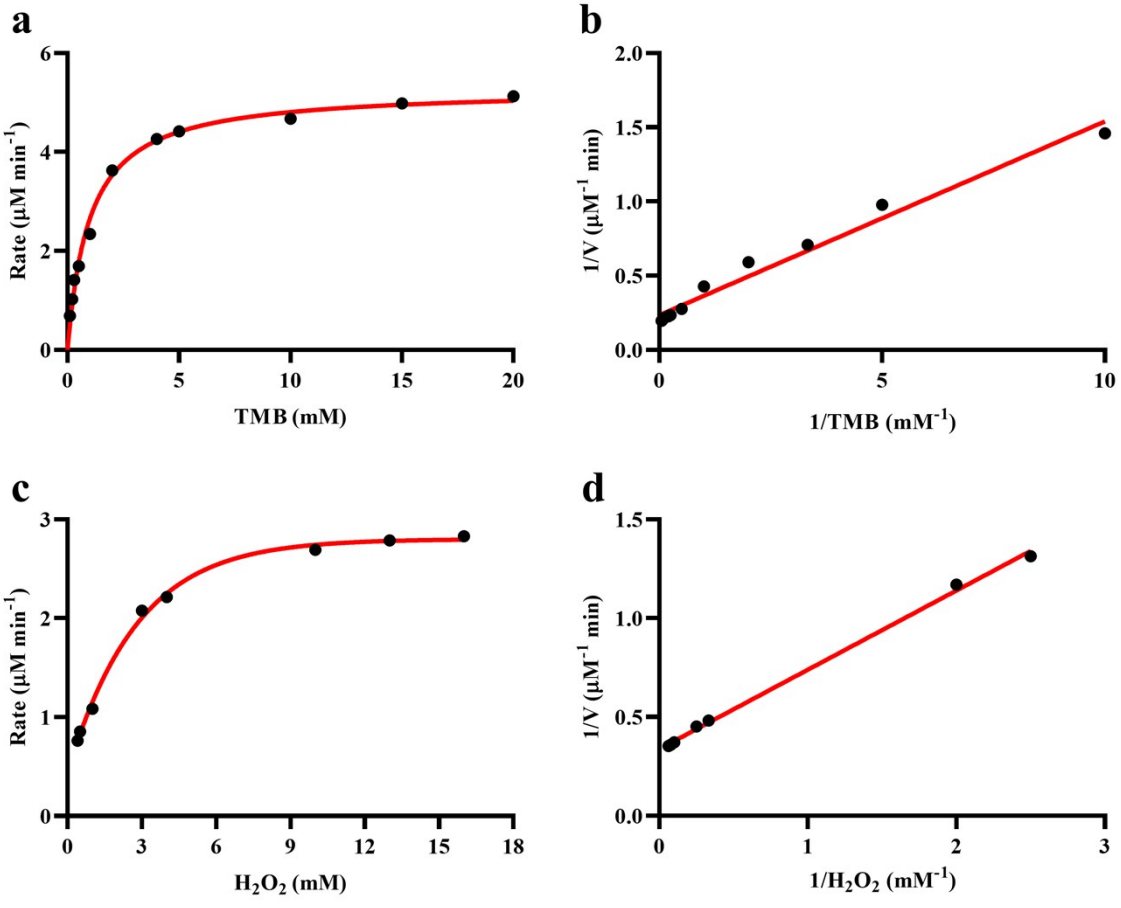

Catalyst	Substance	K_m [mM]	V_{max} [μM min^{-1}]
CuNCs	TMB	0.99	5.28
CuNCs	H_2O_2	1.51	3.09

Fig. S13. The peroxidase-like activity of CuNCs. a) Michaelis-Menten and b) corresponding Lineweaver-Burk plot with various concentrations of TMB (0.1-20 mM) for the CuNCs. Experimental conditions: H_2O_2 (5 mM) and CuNCs (200 μg mL^{-1}) in PBS (10 mM, pH=5.5) at 37 °C. c) Michaelis-Menten and d) corresponding Lineweaver-Burk plot with various concentrations of H_2O_2 (0.4-16 mM) for CuNCs. Experimental conditions: TMB (5 mM) and CuNCs (200 μg mL^{-1}) in PBS (10 mM, pH=5.5) at 37 °C.

Table S1. Comparison of the TON (K_{cat}) and V_{max} values of CuNCs and natural enzymes.

Catalyst	Substrate	[E] (M)	V_{max} (10^{-8} M s^{-1})	TON or K_{cat} (s^{-1})
HRP	H_2O_2	2.5×10^{-11}	8.71	3480
	TMB	2.5×10^{-11}	10	4000
CuNCs	H_2O_2	1.5×10^{-8}	8.8	5.87
	TMB	1.5×10^{-8}	5.15	3.43

Table S2. Comparison of the K_m and V_{max} values of different nanomaterials in peroxidase activity.

Materials	**Substrate**	**K_m (mM)**	**V_{max} (10^{-8} M s^{-1})**	**References**
CuNCs	H_2O_2	1.51	8.8	This work
	TMB	0.99	5.15	
CDs@PtNPs	H_2O_2	0.87	10.2	*Small*, **2020**, 2002348
	TMB	0.079	17.7	
CeO_2 cubes	H_2O_2	30.9	5.75	*Chem. Commun.*, **2020**, *56*, 7897
	TMB	0.180	1.82	
Cu_xO nanocystals	H_2O_2	52.3	23.7	*J. Am. Chem. Soc.*, **2019**, *141*, 1091-1099
	TMB	0.579	38.4	
g-C_3N_4	H_2O_2	4.68	7.23	*Anal. Chem.*, **2017**, *89*, 12327
	TMB	0.56	14.8	
Pt NPs	H_2O_2	206	9.79	*Anal. Chem.*, **2014**, *86*, 10955
	TMB	0.121	6.51	
Co_3O_4	H_2O_2	140.07	12.1	*Chem. Commun.*, **2012**, *48*, 2540-2542
	TMB	0.037	6.27	
Fe_3O_4	H_2O_2	154	9.78	*Nat. Nanotechnol.*, **2007**, *2*, 577
	TMB	0.098	3.44	
Horseradish peroxidase	H_2O_2	3.7	8.71	*Nat. Nanotechnol.*, **2007**, *2*, 577
	TMB	0.434	10	

Table S3. Comparison of the K_m and V_{max} values of different nanomaterials in GPx activity.

Materials	Substrate	K_m (mM)	V_{max} (10^{-6} M s^{-1})	References
CuNCs	H_2O_2	0.097	0.011	This work
	GSH	0.913	0.008	
Cu_xO nanocystals	H_2O_2	0.163	4.91	*J. Am. Chem. Soc.*, **2019**, *141*, 1091-1099
	GSH	1.89	3.13	
Mn_3O_4	H_2O_2	0.196	0.933	*Angew. Chem. Int. ed.*, **2017**, *56*, 14267-14271
	GSH	1.61	1.3	
Graphene Oxide (GO)-Se	H_2O_2	0.04	50	*Chem. Commun.*, **2017**, *53*, 3082-3085
	GSH	0.72	0.82	
V_2O_5@PDA@MnO_2	H_2O_2	0.16	1.46	*Angew. Chem. Int. ed.*, **2016**, *128*, 6758-6762
	GSH	7.2	3.16	
GPx	H_2O_2	0.025	\	*Anal. Chem.*, **2014**, *86*, 11937.
	GSH	10	\	

The symbol "\" represents the value was not determined in the literature.

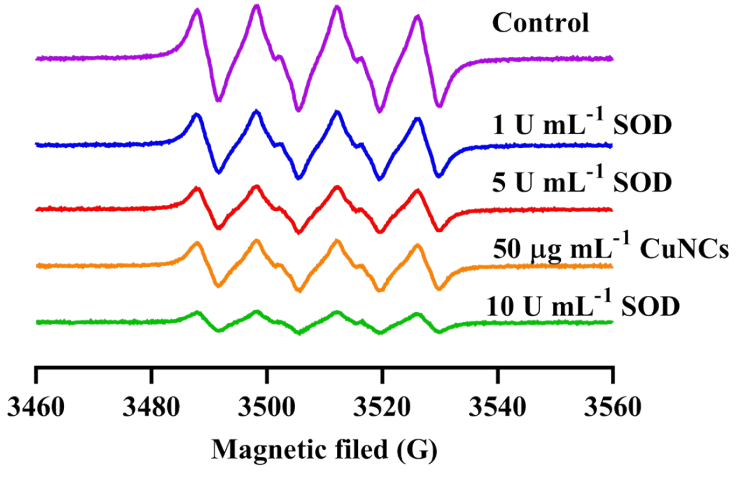

Fig. S14. $O_2^{\bullet-}$ scavenging of CuNCs. EPR spectra were recorded from samples containing xanthine (5 μM), xanthine oxidase (0.5 U mL^{-1}), DMPO (50 μL) and CuNCs (50 μg mL^{-1}) or SOD (1-10 U mL^{-1}). Both SOD and CuNCs can effectively scavenge $O_2^{\bullet-}$, and the scavenging effect of 50 μg mL^{-1} CuNCs can be equivalent to 5U mL^{-1} SOD.

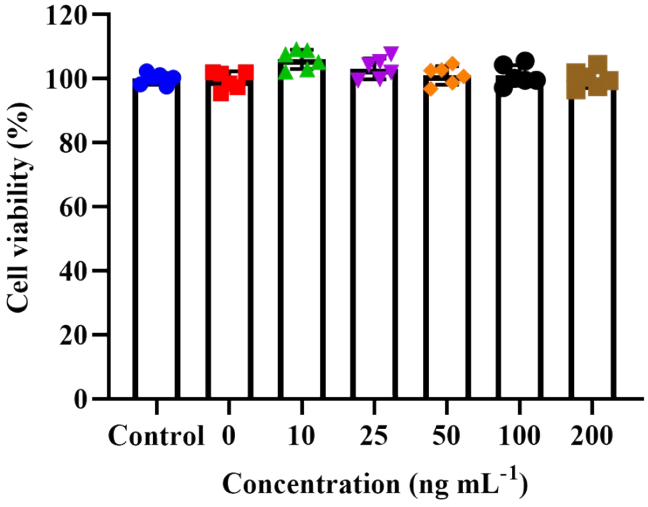

Fig. S15. In vitro cytotoxicity of CuNCs towards HEK 293 cells after incubation for 48 h. There was no decrease in cell viability of HEK 293 cells after incubating with CuNCs for 48 h.

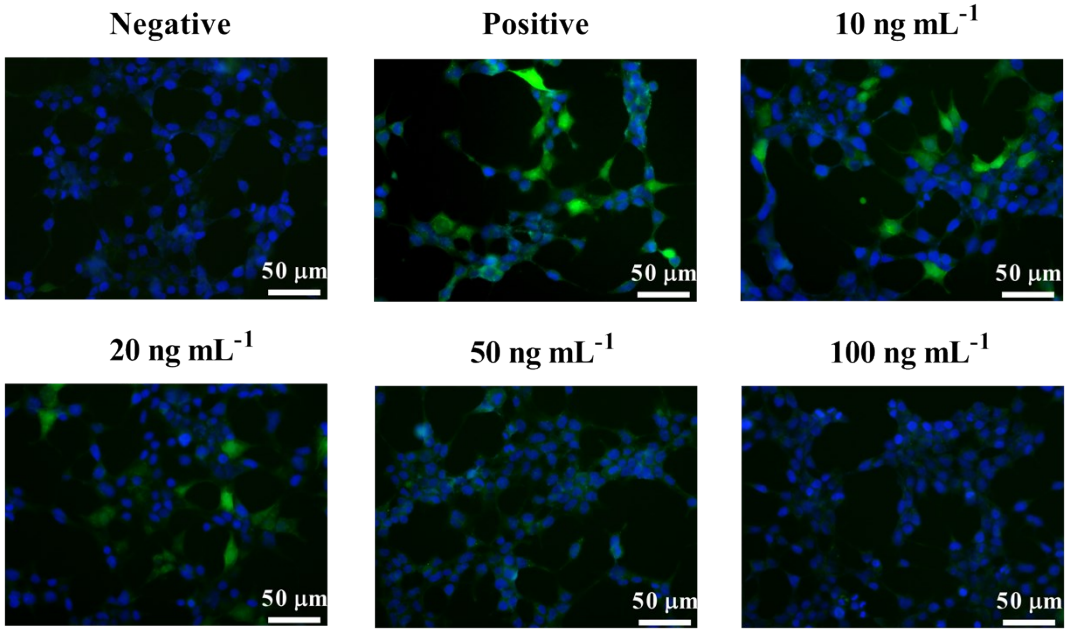

Fig. S16. Colocalization of cells and ROS fluorescence. Negative: HEK 293 cells only. Positive: HEK 293 cells with H_2O_2 (100 μM). Compared with positive group, the ROS signal in HEK 293 cells was significantly decreased after incubation with CuNCs (10, 20, 50, 100 ng mL^{-1}), and were basically eliminated at 100 ng mL^{-1} of CuNCs. Green and blue fluorescence indicated ROS and nucleus, respectively.